Results in Engineering 24 (2024) 103116

Contents lists available at ScienceDirect

Results in Engineering

journal homepage: www.sciencedirect.com/journal/results-in-engineering

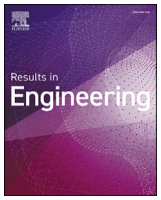

Research paper

A smart, multi-configuration, and low-cost system for water turbidity monitoring

Alessio Vecchio [a,*], Monica Bini [b,c,d], Marco Lazzarotti [b], Marco Luppichini [b], Maurizio Palmieri [a]

[a] Department of Information Engineering, University of Pisa, Via Caruso 16, Pisa, 56122, Italy
[b] Earth Science Department, University of Pisa, Via S. Maria 53, Pisa, 56126, Italy
[c] Istituto Nazionale di Geofísica e Vulcanologia (INGV), Via Vigna Murata 605, Rome, 00143, Italy
[d] Centro Interdipartimentale di Ricerca per lo Studio degli Effetti del Cambiamento Climatico (CIRSEC), University of Pisa, Via del Borghetto 80, Pisa, 56124, Italy

ARTICLE INFO

Keywords:
Turbidity
Sensor
Environmental monitoring

ABSTRACT

Measuring the amount of suspended sediment in rivers is important for a better understanding of phenomena like soil erosion or floods. Since such phenomena are not spatially homogeneous, a distributed measurement approach is required to obtain fine-grained and realistic models. We designed and implemented a low-cost, flexible, and smart suspended sediment concentration monitor. The system only uses components that are easy to find and assemble. This, together with the reduced costs, enables the use of multiple instances for distributed monitoring. The system can operate according to different configurations, fixed or mobile, and using a variety of connection technologies, to possibly cover the various necessities that arise from the diverse installation sites. Each measuring unit automatically retrieves its operational parameters, easing the configuration of a possibly large distributed measurement system.

1. Introduction

Suspended sediment in rivers plays a significant role in both ecological health and human activities, making its measurement crucial. Sediment originates from natural processes like soil erosion and human operations such as construction and agriculture. High levels of suspended sediment reduce water quality, harm aquatic life, and increase water treatment costs. Accurate and reliable measurement of suspended sediment concentration (SSC) in rivers is essential for effective environmental monitoring, water resource management, and regulatory compliance. Measuring the amount of suspended sediments is also important to model natural erosion phenomena, or to better estimate the amount of material brought by rivers into the sea. Traditional methods for measuring SSC, such as gravimetric analysis, involve collecting water samples and then processing them in a laboratory. While these methods are accurate, they are labor-intensive, time-consuming, and impractical for real-time monitoring. More practical approaches are based on measurements of the water turbidity, as the presence of suspended sediment influences the latter. The basic idea is to illuminate the water sample using a controlled light and measure both the attenuation and the amount of light reflected by the suspended particles. In particular, the light scattered by particles is measured using photodiodes placed at different angles with respect to the incident light. The use of multiple photodiodes generally increases the accuracy of measurements and provides robustness against the different particle sizes. An instrument that measures the amount of suspended particles using a side-placed photodetector is also known as a nephelometer.

Recent literature highlighted the importance of monitoring the amount of suspended sediment frequently and in a distributed fashion, in order to capture the details of the phenomenon from multiple points of view and in the end obtain models that are more realistic and fine-grained [1]. For instance, accurate hydrogeological models concerning sediment transportation need data about SSC dynamics during intense precipitation events, requiring multiple measurements in a short timeframe. The data also has to be spatially distributed, to avoid the possible bias introduced by a single specific measurement site. These needs gave rise to an increasing research body about low-cost distributed SSC measurement systems, motivated by the high cost of commercial off-the-shelf turbidimeters that can be in the order of a few thousand euros.

When turbidity is measured through diffused radiation, the level is expressed in Nephelometric Turbidity Units (NTUs) or in Formazine Nephelometric Units (FNUs) [2]. Formazine is a polymer that is poorly soluble in water and it is used for calibration of turbidimeters. Turbid-

* Corresponding author.
E-mail address: alessio.vecchio@unipi.it (A. Vecchio).

https://doi.org/10.1016/j.rineng.2024.103116
Received 7 August 2024; Received in revised form 28 September 2024; Accepted 11 October 2024
Available online 17 October 2024

ity can then be converted into SSC using a site-specific scale, since their relationship depends on sediment properties (see, for instance, the different coefficients used in [3] and [4] because of the characteristics of the considered streams). The relationship between SSC and turbidity was studied in North-Western European streams, looking for correlation patterns based on stream characteristics, such as catchment area, land use, or soil type [5]. Results show that preparing a calibration curve between turbidity and SSC for each river is fundamental and that harmonizing the methods across countries is necessary. This necessity is also backed by [6], where a comparison between twelve commercially available turbidity sensors highlights that the variability of the instruments can hinder the transferability and comparability of datasets acquired by different regulatory agencies. If the final goal of the system is to estimate SSC, then calibration can be directly carried out from the raw readings provided by the photodiodes to SSC values.

We present a smart, multi-configuration, low-cost turbidimeter useful for in-site SSC measurements. The turbidimeter

- has a reduced cost allowing the use of multiple units for distributed measurements;
- is built using only off-the-shelf components and does not require any custom Printed Circuit Board (PCB);
- supports multiple configurations, as it can operate in mobile or fixed mode, and can communicate via wireless and wired setups;
- is smart, as it is able to retrieve its operational parameters from a server, and reliably transfer collected data to a remote site;
- can be easily replicated, as all the software is open-source and publicly available.

The remaining of this work is organized as follows: Section 2 provides an analysis of related work on low-cost sensors for turbidity measurement, Section 3 shows the overall system, Section 4 describes the elements of the turbidimeter, including the list of materials, Section 5 discusses the performance of the sensor achieved during laboratory tests, Section 6 presents the architecture of the server that manages the turbidimeters and collects their data, Section 7 discusses how a flexible approach can be helpful in turbidity monitoring, and finally Section 8 concludes this work.

2. Related work

A review of the principles of turbidity measurement can be found in [7]. Laboratory tests aimed at comparing acoustic and optical sensors for SSC measurements showed that, for non-homogeneous solutions, the optical approach is generally more accurate [8]. The impact of different optical configurations on the accuracy of turbidity sensors is evaluated in [9].

In [10], a turbidimeter based on infrared (IR) and RGB light (the latter is useful to obtain information about the color of the sample) was used to observe the presence of phytoplankton in marine water. The turbidimeter exported collected data using a satellite connection and a mail server. Another low-cost sensor for seawater quality, based on blue and red light and designed to measure chlorophyll and turbidity continuously, is described in [11]. In [12], a low-cost turbidimeter for water quality monitoring in fish farms uses four LEDs with different wavelengths to distinguish sediment from phytoplankton. Another turbidimeter designed to be used in situ combines two photodetectors and two infrared light sources to measure both scattered and attenuated light according to a ratiometric method [13]. In [14] a cost-effective turbidity sensor is designed, tested, and later embedded in a maritime station for real-time and online monitoring of the coastal area [15]. A device for in situ estimation of suspended sediment transport using measurements of water velocity, sediment concentration, and depth is described in [16]; data collected by the sensor was logged onto a device placed outside the water using a cable and the RS485 protocol. In [17], a low-cost sensor with eleven LEDs and three photodiodes is proposed for real-time water monitoring, using the GSM communication method for data extraction and alert management. A turbidity and particle size sensor based on a single-photon detection technique is proposed and analyzed in [18] achieving an adjusted R^2 value of 0.99. Although the sensor is small, the authors do not mention its usage for river monitoring.

According to [19], the most common range for water turbidity analysis is 0.1-1000 NTU. For example, drinking water must not exceed 1 NTU, river water can reach 150 NTU, and wastewater is about 1000 NTU. In [20], the authors propose the design of a low-cost turbidity sensor for fresh-water courses, achieving an accuracy of 0.1 NTU resolution in the 0-200 NTU range and 1 NTU resolution in the 0-1000 NTU range. Details on the wireless connection capabilities of the sensor are not reported. The analysis of an off-the-shelf turbidity sensor is presented in [21], along with a custom design to overcome its limitations. The custom design exhibits reliable measures in the range of 100-4000 NTU. A different approach for low-cost water turbidity sensing is proposed in [22], where four optical fibers are used to convey the rays of light traversing a fluid to the rear camera of a smartphone. Another smartphone application for water turbidity measurement is proposed in [23]; this application requires a smartphone equipped with standard sensors (gyroscope and compass) to take photos of the water surface from different angles. Another approach for water turbidity measurement involves the processing of images collected by Unmanned Aerial Vehicles (UAVs) while flying above rivers [24]; this approach still requires in situ turbidity sensors to validate the results obtained with images. Similarly, approaches based on satellite images still require in situ turbidity sensors for ground measurements as in the case of [25]. Another technique for water quality assessment, based on microwave analysis, is proposed in [26]. Finally, a high-speed recording camera (80 frames per second) was used to evaluate the interaction of two colliding currents with different turbidity levels [27]. An open-source turbidity sensor is presented in [1]. The turbidimeter is based on an LED and two sensors controlled by a Micro Controller Unit (MCU). The system was later improved in [28], using an Arduino MKR WAN 1310 and with a total cost of roughly 200 EUR. The CAD files for 3D printing the head of the turbidimeter, as well as the schematics needed for the production of the PCBs hosting the photodiodes, were made available according to an open-source license. In [29], a Wixel board controls the sensor, and the data is logged on a Raspberry Pi, with an overall cost of 550 EUR.

The increased availability of historical data is now fostering the adoption of machine learning techniques, such as Artificial Neural Networks or Exponential Gaussian Process Regression, to generate models for sediment transport prediction [30,31].

The sensor proposed in this work is mostly inspired by [1,28]. Our turbidimeter enhances existing systems by easing the production and customization of the device, which is completely built using off-the-shelf components and it does not rely on any custom PCB. In addition, the system we propose includes enhancements in terms of connectivity and usage options, as it can be effortlessly configured to operate in fixed or mobile settings using wireless and wired setups for communication. The system can also be configured from a remote site, e.g. to tune its operational parameters depending on weather conditions or other environmental factors.

3. Overview

The principle of operation of the turbidimeter is illustrated in Fig. 1. An LED is used to illuminate the water. Two photodetectors are placed at 90°and 135°, to measure the amount of light scattered by the suspended sediment in the water. The LED emits light in the infrared (IR) band, in particular using an 850 nm wavelength. The use of a wavelength greater than 800 nm reduces the interference due to the natural color of water caused, for instance, by humic substances [7]. The two photodetectors are actually made by a couple of photodiodes each. The two photodiodes at each collection point operate according to different response curves in the visible and IR frequency ranges. So, in the end,

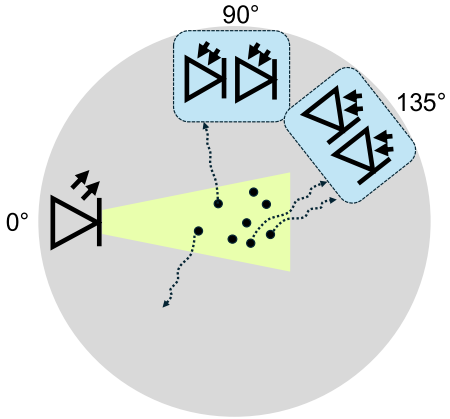

Fig. 1. Principle of operation: an IR LED emits light scattered by the particle suspended in water. Light is measured by two photodetectors. Each photodetector is made of two photodiodes operating at different frequency bands.

four light measurements are available, increasing the accuracy of the device.

The optoelectronic subsystem is controlled by a Single Board Computer (SBC) that runs the sampling logic and locally stores the results. The SBC uses a communication subsystem to interact with an external server. The external server provides the turbidimeter's current operational configuration and stores the results of measurement operations in a database. Two different communication configurations are available: the mobile one and the fixed one. The configuration also determines how power is provided to the system: in the mobile configuration power is provided through a battery, whereas in the fixed configuration power is provided through a cable. The two configurations allow the turbidimeter to be used in different scenarios. The mobile configuration is supposed to be used when the measurement site is far from ICT infrastructure or when mobility provides an additional measurement dimension. It allows, for instance, to measure the turbidity of a river longitudinally using a boat or transported by the water flow. The fixed configuration is supposed to operate close to ICT infrastructure and it allows sending of collected data in real-time. In addition, it is not energy-constrained, so it is possible to increase the sampling frequency above the rates that are possible when battery-operated.

The idea of directly connecting to existing infrastructure originated from the possible presence of other instrumentation along the stream to be monitored. In urbanized areas, rivers are frequently monitored through fixed infrastructure, for example to measure the water level. Such measurement infrastructure is generally powered using cables, and Internet access can be available as well. We hence identified Power-over-Ethernet (PoE) as a technology able to provide both connectivity and power to the device. A PoE-enabled switch has a very limited cost and the installation just requires putting the PoE-enabled switch between the turbidimeter and the existing Internet connection. ICT infrastructure, on the other hand, is less likely to be present in minor rivers or less urbanized areas. In those situations, the wireless configuration, possibly based on a cellular connection, can be the most reasonable choice. If no cellular coverage is available, the turbidimeter still stores internally all the readings and uploads them to the server as soon as Internet access is available.

The overall system is represented in Fig. 2. The head of the turbidimeter hosts the LED, the photodiodes, and the optics.

4. Design and materials

This section describes the design and materials of the different parts of the turbidimeter.

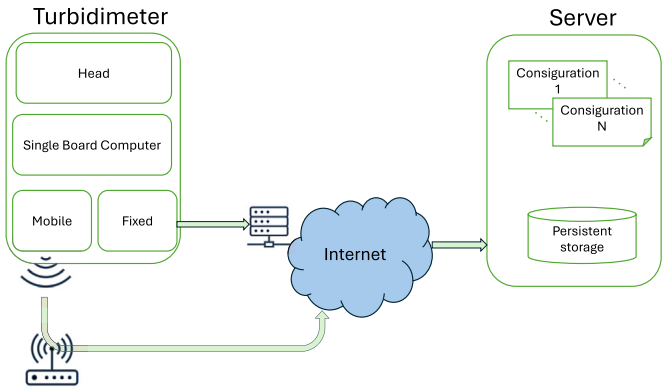

Fig. 2. The Head of the turbidimeter hosts the IR LED, the photodetectors, and the optics. The Single Board Computer controls the head of the turbidimeter and communicates the results to a remote server. The turbidimeter can operate in a mobile configuration, where access to the public Internet is achieved via Wi-Fi or cellular connection, or in a fixed configuration, where connectivity is achieved through a switch. Arrows show the way turbidity information is transferred, configuration information goes in the opposite direction.

4.1. Head

The head of the turbidimeter hosts the TSHG6200 850 nm LED emitter and two TSL25911FN ambient light sensors. Each sensor transforms light intensity into a digital value provided via I2C. Each sensor is equipped with one broadband photodiode (visible plus IR) and one IR-responding photodiode. So there is a total of four light sampling values for each turbidity reading: two from the broadband photodiodes at 90°and 135°, and two from the IR-responding photodiodes, at 90°and 135°. The head has been 3D-printed, starting from the CAD files proposed in the supplementary material of [28]. The two light detectors are placed at 90° and 135° with respect to the emitter as this configuration proved to be better than others (as reported in [1] where multiple configurations were compared). We modified the original CAD files to host the boards, made by CQRobot/Waveshare, containing the TSL25911FN ambient light sensors, which are larger and with a different form factor, and to align the photodiodes of the board with the holes used for receiving the light. We also designed a 3D-printable plate that can be used to close the back of the head (we preferred this solution to the alternative solution of filling the head with epoxy resin, as the latter option is non-reversible). Two lenses (characteristics detailed in Table 1) are used to focus the light onto the TSL25911FN photodiodes and to isolate them from the water. A third lens was used for the LED (characteristics in Table 1). Since 3D-printed components are not waterproof, the head of the turbidimeter was covered with epoxy resin. Lenses were glued to their housing again using epoxy resin. The head, both open and attached to the body of the turbidimeter, is shown in Fig. 3.

4.2. Main logic and body

The logic of the device is executed by a Raspberry Pi Zero WH Single Board Computer. The Raspberry Pi controls the LED and the light sensors. The Zero WH variant has been chosen for its compact size, reduced power consumption, wireless connectivity, and the presence of an already soldered General Purpose Input Output (GPIO) connector (in this way, no soldering is needed to connect the LED and the sensing boards). The Zero WH shares with other Raspberry devices the Debian-based Raspberry Pi OS which allows the definition of the operation logic using high-level programming languages, mostly Python and shell scripts. In addition, being a Linux-based system we were able to set up a synchronization mechanism using a utility that is commonly available on Unix-like systems (rsync). In particular, sensor readings are immediately locally saved onto a micro-SD card. The device performs a periodic synchronization of the local data with a remote site. Only

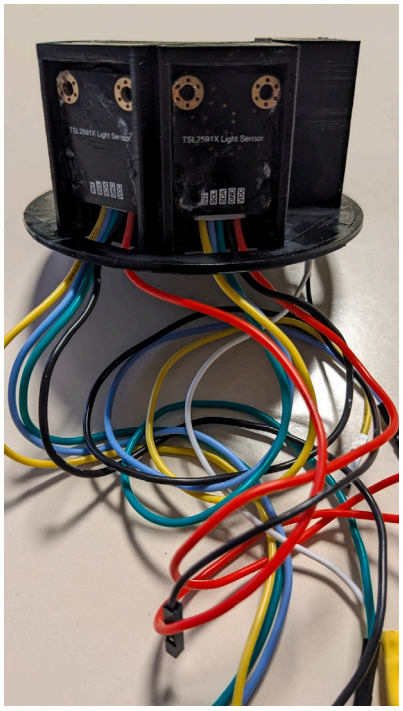

(a) Head of the turbidimeter with the boards hosting the light sensors. The 3D-printed head is an adaptation of [1], modified to host the ready-to-use boards.

(b) The mobile version of the turbidimeter placed onto its wireless recharge station (the round base with a green light). The turbidimeter is ∼17 cm high, with a diameter of ∼10 cm. The cable is a standard USB-C cable that provides power to the charging station.

Fig. 3. Head of the turbidimeter and a complete mobile prototype.

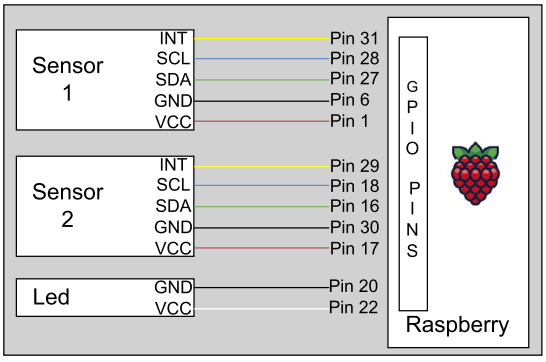

Fig. 4. Wiring between the optical components and the board.

changes with respect to previous synchronizations are transferred, in order to reduce the amount of data to be sent and, in turn, also the energy spent. In case of a connection failure, data is not lost and turbidity readings will be transferred when the next successful synchronization occurs. Furthermore, the operating system hosts an ssh daemon. This makes it possible to log into the turbidimeter from a remote computer, for example to troubleshoot sensor malfunctions or to update the controlling software. Overall, the high-level mechanisms provided by the Linux-based operating system, including its libraries and tools, led us to choose this type of board instead of other solutions based on MCUs.

The optoelectronic components are connected to the GPIO pins of the Raspberry board according to the schema shown in Fig. 4. A resistor (100 Ω) is inserted between the Raspberry Pi and the LED to limit the maximum amount of current across GPIO pins. The boards hosting the TSL25911FN sensors cannot be configured to use a designer-defined I2C address. To avoid a collision on the I2C bus, we had to set up a secondary I2C bus so that the two boards could use the same address on their own dedicated bus.

Whenever a measurement has to be carried out, the four photodiodes are read with the LED turned off and then again with the LED turned on. Readings with the LED turned off allow us to obtain information about the amount of environmental light, which can be useful to increase the accuracy of the device. This procedure is repeated n times, back to back, to obtain statistically meaningful results. The default value of n is five, so there are five raw samples with the LED on and five with the LED off at each measurement time. The value of n can be changed using the turbidimeter's configuration file.

We decided not to 3D print the housing of the electronic part of the turbidimeter and to use instead a polypropylene tube. Polypropylene tubes used in construction are commonly available, they are waterproof, and already equipped with O-rings. A polypropylene tube is also cheaper than a 3D-printed case, which in addition needs to be covered in epoxy resin to be made waterproof. The only problem with polypropylene is its limited bonding with epoxy resin. For this reason, the head of the turbidimeter has been glued to the tube using a silicone adhesive. Closing the tube with its cap also needs some care: since the system is airtight, the internal pressure increases as the cap is inserted into the tube. The internal pressure can be so high to pop the lenses of the turbidimeter from their housing. To avoid this problem, we made a small hole in the bottom cap, to allow the air to flow out when the cap is closed. Then the hole is sealed with a small amount of silicone. This procedure has to be carried out only during the assembly phase since the turbidimeter can be charged without the need to open it, as discussed later.

The following subsections show the two possible configurations: the mobile one and the fixed one. The advantages and drawbacks of the two configurations are also highlighted. Each configuration has its own set of

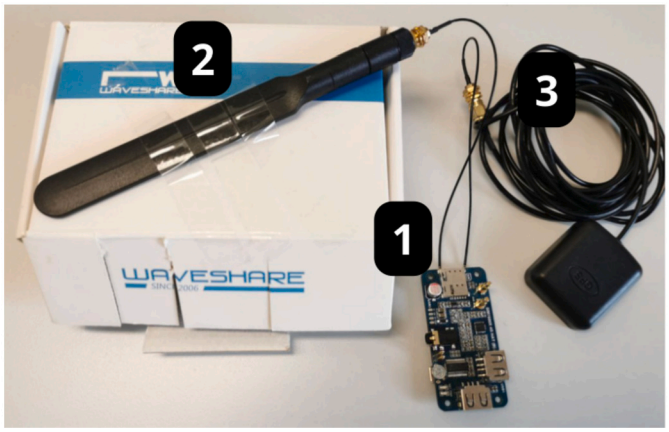

Fig. 5. 1: LTE module, 2: LTE antenna, 3: GPS receiver.

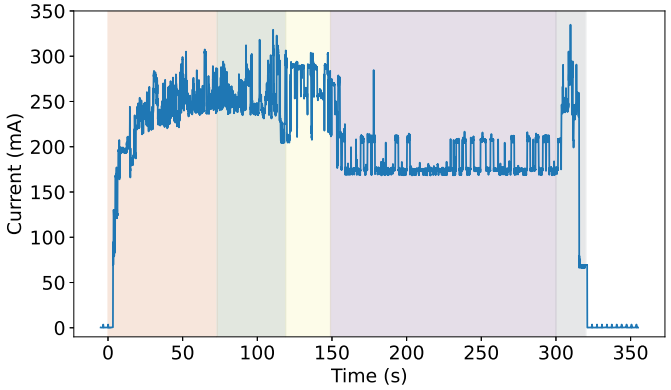

Fig. 6. Current absorbed during a complete operational cycle. Communication takes place via Wi-Fi, using a smartphone as a hotspot. The different operational phases (boot, measurement, synchronization, idle, and shutdown) are highlighted using different colors.

additional components with respect to what has been already included in the head and body of the turbidimeter. Immediately after the boot phase, the turbidimeter looks for a configuration file that details the current mode of operation, mobile or fixed, and other relevant parameters, such as the communication technology (Wi-Fi, cellular, or Ethernet) and the sampling period. Table 1 shows the list of materials and the related prices for all the considered components.

4.3. Mobile configuration

The Raspberry Pi Zero WH natively supports Wi-Fi communication. The turbidimeter can be configured to look for an access point with a given name and to automatically connect to it. This first option can be useful in two scenarios: i) the turbidimeter is placed in an area covered by Wi-Fi (as it may happen in urban settings); ii) an operator moves close to the turbidimeter and uses a smartphone as a hotspot (to this purpose it is sufficient to give the hotspot a well-known name and password). If Wi-Fi is not the most suitable wireless technology, cellular communication can be used. For this purpose, we used a SIM7600X 4G HAT LTE module. The SIM7600X 4G HAT, its antenna, and the GPS receiver are shown in Fig. 5. The cellular subsystem, including its antenna, is enclosed in the same polypropylene tube where the Raspberry Pi is contained. Note that when the turbidimeter is submerged, neither Wi-Fi nor cellular communication is possible, as communication is blocked by water. The idea is that the turbidimeter locally stores sampled values and transmits them at the next synchronization window, when it is manually extracted from the installation site or if it emerges because the level of water gets lower, e.g. after the intense precipitation event to be monitored. Another possibility is to connect the 4G HAT via a USB cable, so that the head and main body of the turbidimeter are submerged, whereas the cellular board and the antenna are placed above the surface. This solution requires the use of a sealing element like the one adopted in the fixed configuration. The GPS receiver is automatically turned on, if enabled in the configuration file, to enrich the turbidity readings with the current device position. This can be useful when moving during a measurement campaign.

We experimentally evaluated the energy consumption of the main operational phases of the device. For this purpose, we used a smart power monitor, which is able to power the device under test and, at the same time, measure accurately the current provided. In particular, we used an Otii Ace Pro configured to collect 10 K samples per second and with an accuracy of $\pm(0.05\% + 25\text{nA})$. To accurately collect the duration of the main operational phases we used one of the GPIO pins of the Raspberry Pi. The status of the pin was toggled via software at the end of the boot, measurement, synchronization, and idle phases. The status of the pin was sampled using an input port provided by the Otii Ace Pro, obtaining an auxiliary trace that was used to segment the power trace. Fig. 6 shows the current absorbed by the Raspberry Pi. The device executes the boot, measurement, and synchronization phases. The latter is carried out using Wi-Fi and a hotspot provided by a common smartphone. The device was configured to start the shutdown sequence after 300 s from the beginning of the boot phase. So, after synchronization, the device remains idle until it is time to power off. Fig. 6 highlights the different phases using different colors. We collected five execution traces. The mean and the standard deviation of the duration and consumption of main phases are provided in Table 2. The evaluation was limited to five executions as we noticed the times and the absorbed current were fairly stable. The boot phase has a duration of approximately 73 s. The boot phase also contains the activation of the Wi-Fi interface and connection to the hotspot. During the measurement phase, the device collects five measurements with the LED on and five with the LED off (intertwined). The measurement phase also includes writing collected data on the local filesystem. The synchronization phase is the most energy-hungry, because of communication. Once synchronization is finished, the device remains idle. This period can be trimmed in production devices to save energy. During the evaluation experiment, we included such an idle phase to estimate the energy cost of keeping the device powered on. Keeping the device turned on can be useful for remotely connecting to the device in case of a partial malfunction or for updating the onboard software (note that the device can accept incoming connections only after the boot phase). At time 300 s, the Raspberry Pi starts its power-off sequence, which is completed in ~ 17 s.

In related studies (e.g. [28]), one measurement per hour is considered a suitable rate for fluvial turbidity analysis. Starting from this assumption, and considering that the device is powered by a 10000mAh LiPo battery, we can get an estimation of the lifespan of the device. If the device remains always turned on and carries out one measurement and synchronization per hour, the average current needed would be ~ 189.3 mA (45.1 s at 253.1 mA, then 25.1 s at 279.4 mA, and ~ 3530 s at 187.8 mA). The device lifetime would be: 10000 mAh/189.3 mA $\approx$53 h.

To increase the lifespan of the device, a Witty Pi 4 L3V7 HAT has been mounted on top of the Raspberry board, to periodically turn on and off the system. The Raspberry Pi Zero, in fact, does not include a real-time clock, and once powered off it is unable to self-start. This possibility is provided by the Witty Pi board, which stores the current time and restarts the Raspberry Pi according to a configurable schedule. The Witty Pi allows us to set the switching period between these two states with a simple syntax, shown in Listing 1, that defines the range of validity of the schedule (from the BEGIN date to the END date), the amount of time in the ON state and the amount of time in the OFF state. In practice, thanks to the Witty Pi schedule, it is possible to periodically sense the turbidity of water and then turn the device off. This increases the device's lifetime because the consumption in the sleeping state is

Table 1
Summary of the required materials and their costs.

Material	Cost (EUR)
Core components	
TSL25911FN light sensor, board made by QRobot or Waveshare	8.4 × 2
TSHG6200 LED emitter	1
Plano-convex lens (diameter = 6 mm, focal length = 14.9 mm), from Thorlabs	20.5 × 2
Plano-convex lens (diameter = 6 mm, focal length = 10.0 mm), from Thorlabs	21.9
Raspberry Pi Zero WH	18
Polypropylene EN 1451 tube and caps (O-ring included), from a local hardware supplier	8
3D-printed head	8
TOTAL of core components	114.7
Mobile configuration components	
Witty Pi 4 L3V7 HAT	24
LiPo Battery 10000 mAh	29
Wireless charge receiver	5
SIM7600X 4G HAT + GPS receiver + LTE antenna (needed only for cellular access)	70
TOTAL of mobile configuration components	128
Fixed configuration components	
Waveshare PoE Hat	27
Ethernet cable, 20 meters, cat. 6	20
Compression gland WetLink Penetrator, Blue Robotics	12
TOTAL of fixed configuration components	59

Table 2
Duration and consumption of the main operational phases.

Phase	Mean duration ±st.dev.(s)	Mean current ±st.dev. (mA)
Boot	72.7 ± 1.5	233.4 ± 0.5
Measurement	45.1 ± 1.0	253.1 ± 1.0
Synchronization	25.1 ± 0.6	279.4 ± 4.7
Idle	156.5 ± 0.9	187.8 ± 1.1
Shutdown	17.2 ± 0.3	196.6 ± 3.3
All	316.6 ± 0.5	215.3 ± 0.8

significantly smaller.[1] On average, the device would require 242 mA during the boot, measurement, synchronization, and shutdown phases (we here suppose that the idle phase is not required). The total duration of such phases is ∼ 160 s. The lifespan, in this case, would be ∼ 39 days.

It is important to note that obtaining a longer lifetime is not particularly useful: the turbidimeter, in its current version, is not equipped with a lens cleaning system, and the fouling accumulating over time onto the optics would make the measurements unreliable. For example, according to in situ tests performed in [32], a sensor based on optic elements shows a measurement drift after one week of seawater exposure. To extend the lifetime of the device, anti-biofouling techniques would be required (e.g. the ones described in [33]).

```
# Turn on for 4 minutes, every 60 minutes
BEGIN 2021-08-07 00:00:00
END   2025-07-31 23:59:59
ON    M4    # Keep ON state for 4 minutes
OFF   M56   # Keep OFF state for 56 minutes
```

Listing 1: Scheduling syntax.

Using a cellular access network and the GPS requires additional energy compared to Wi-Fi communication, because of the higher power absorption of the LTE modem and the energy spent to obtain a GPS fix. Using the power monitor, we experimentally evaluated also the energy needed by the turbidimeter when the cellular HAT is included in the configuration. The average current, during a cycle like the one detailed in Table 2, increases of ∼ 60 mA compared to the Wi-Fi solution.

The LiPo battery can be recharged without opening the waterproof enclosure. In particular, a wireless power receiver is placed internally, attached at the bottom of the tube. Then, it is sufficient to place the turbidimeter on top of a common wireless charging station, like the ones used to recharge smartphones, to transfer energy to the inner side of the device.

The cost of a mobile turbidimeter goes from ∼173 EUR (Wi-Fi only) to ∼243 EUR (with also cellular access and GPS receiver). The mobile version weighs ∼ 520g (including the 155 g battery) and has a volume of ∼ 1.5 L. Thus, the turbidimeter floats unless it is fixed to some underwater support or weight is artificially added.

4.4. Fixed configuration

The fixed configuration is based on the Power-over-Ethernet (PoE) technology. PoE allows using a single cable for communication and power. This is particularly useful because just one cable exits the body of the turbidimeter, which must be waterproof. We used a Waveshare PoE Hat placed on top of the Raspberry Zero board to extend it with an Ethernet port that supports the PoE 802.3af standard. The Ethernet cable enters the body of the turbidimeter through a compression gland (WetLink Penetrator) designed for underwater robotics. This configuration provides underwater connectivity and unconstrained energy. As a consequence, there is no need to power off the turbidimeter and it can carry out SSC measurements at higher rates compared to the mobile configuration. The major drawback of this solution is the need for ICT infrastructure nearby, specifically a PoE-enabled switch.

The cost of a fixed turbidimeter is ∼174 EUR. The fixed version weighs ∼ 365 g and has a volume of ∼ 1.5 L. Thus, also in this case, the turbidimeter floats unless it is fixed to some underwater support or weight is artificially added.

5. Sensor calibration

We calibrated one of the turbidimeter prototypes using three different types of sediment. For each type, we prepared water samples with different, and well-known, concentrations of suspended sediment. During the measurements, each water sample was continuously agitated using a magnetic stirrer. The turbidimeter was calibrated directly against concentrations of suspended sediment. We did not calibrate the turbidimeter using formazine since turbidity values should be later converted in SSC using a site- and flow-specific scale. In addition, formazine is carcinogenic, thus avoiding such a step is an added value, as also highlighted in recent literature. The samples used for calibra-

[1] The current needed during the off periods, measured using the power monitor, is ∼ 345 μA.

Table 3
Characteristics of the samples used in the calibration.

Sample	Min conc. (g L^{-1})	Max conc. (g L^{-1})	Munsell color sys. (dry)	Munsell color sys. (wet)
1	0.5	8	2.5Y 7/2	2.5Y 4/2
2	0.5	7	2.5Y 6/3	2.5Y 4/2
3	0.25	7	2.5Y 6/1	2.5Y 3/1

Table 4
Sensors used for the different cases considered in the regression analysis.

	Emitter condition	LED ON				LED OFF			
	Photodetector Angle	90°		135°		90°		135°	
	Photodiode	IR	IR+Visible	IR	IR+Visible	IR	IR+Visible	IR	IR+Visible
Case	All parameters	x	x	x	x	x	x	x	x
	90° light detector	x	x			x	x		
	135° light detector			x	x			x	x
	LED on	x	x	x	x				
	LED off					x	x	x	x
	IR	x		x		x		x	
	IR+Visible		x		x		x		x

Table 5
Error metrics of the sensor calibration.

Case	Adjusted R-squared	R-squared	RMSE (gL^{-1})	MAE (gL^{-1})
All parameters	0.97	0.94	0.55	0.26
90° light detector	0.93	0.79	1.07	0.88
135° light detector	0.94	0.83	0.97	0.74
LED on	0.96	0.88	0.79	0.45
LED off	0.54	-0.29	2.64	4.01
IR	0.93	0.80	1.04	0.77
IR+Visible	0.94	0.82	0.99	0.72

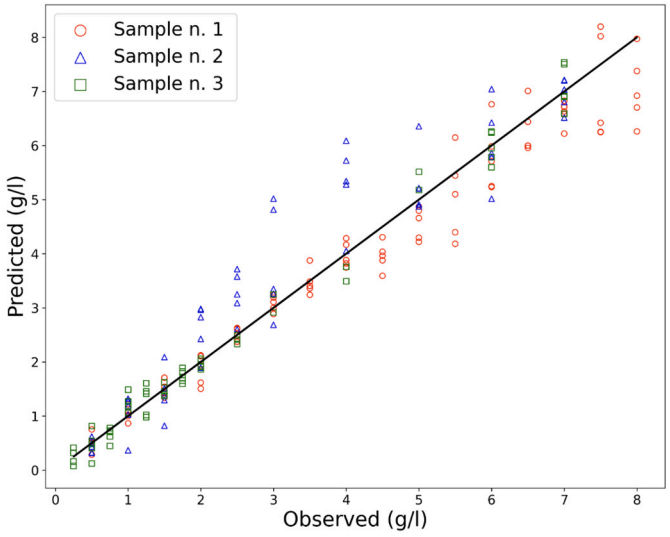

Fig. 7. Calibration of the turbidimeter.

tion were characterized by a granulometry below 63 μm,[2] as it is the principal component in suspended transported sediment in rivers. The sediment used for the calibration was collected from the Arno River (Italy), where the turbidimeters operate. The Arno River is characterized by rapid runoff, with bank-full events occurring within a few hours, making it necessary to intensify SSC monitoring during relatively short time frames. The three sediment samples have slightly different colors as detailed in Table 3. We started from 0.25-0.5 gL^{-1} concentrations up to 7-8 gL^{-1}. The higher end of the chosen range corresponds to the concentration that is typically reached during intense flow events for the considered river. Measurements have been carried out with different environmental conditions, in terms of lighting, due to random use of artificial lighting, the time of the day, weather conditions, and the orientation of the photodiodes relative to the external light sources. Collected data have been used to obtain a regression curve according to the Ordinary Least Squares method. Besides the raw readings of the sensors, we used as input of the method the difference between parameters, the ratio between parameters, and the square of parameters. By adding these transformations, the model can capture more complex and nonlinear relationships between the data. These operations highlight interactions that a simple linear regression might miss, such as proportions, quadratic effects, or subtle variations. This expands the model's ability to identify hidden nonlinear patterns in the variables. Such enrichment of the parameters as the input of the methods was fundamental to obtain significantly better results. Fig. 7 shows the result for the three samples. Overall the calibration is remarkably accurate, with Adjusted R-squared equal to 0.97, R-squared equal to 0.94, RMSE equal to 0.54 g L^{-1}, and MAE equal to 0.26 g L^{-1} (Table 5). Additional regressions were conducted examining the role of the different light detectors, using only the LED on or off readings, or using only IR readings or only IR+Visible readings, according to the cases defined in Table 4. The goal is to understand the role of the different elements in terms of accuracy. Using the sub-datasets, the performances are lower and the results indicate that the main role is played by the IR LED (Table 5). When we use only the parameters acquired with the LED off, the calibration is not efficient (case LED off in Table 5). This suggests that the use of the IR LED improves accuracy by reducing the influence of environmental conditions.

When using just one of the two photodetectors (90°light detector or 135°light detector cases in Table 5) the accuracy is approximately the same. Their combined use however provides significantly better results. The IR-only case uses just the infrared-responding photodiodes. Accuracy is significantly lower compared to the usage of all the four

[2] 63 μ*m* is the upper limit of the *coarse silt* size range, according to ISO 14688.

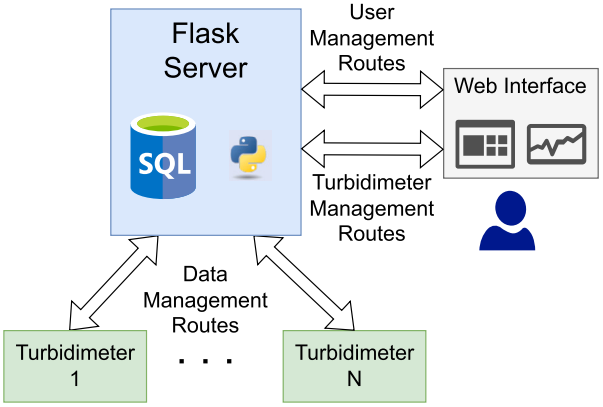

Fig. 8. Schema of the Flask Server.

photodiodes. The same happens for the IR+Visible case. In the end, both the spatial placement of sensors and the use of photodiodes operating at different frequency bands contribute to the accuracy of the system.

6. Back-end

The server has three primary functions: i) data collection from all the deployed turbidimeters, ii) data presentation through a simple Web interface, and iii) hosting of turbidimeters' configuration files.

The server exploits the Flask framework and relies on a MySQL database for data persistence. The server defines three categories of Flask routes: User Management Routes, Turbidimeter Management Routes, and Data Management Routes. The User Management Routes handle tasks like registration and login of users. Turbidimeter Management Routes handle operations like adding/removing a new turbidimeter to the system and modifying a turbidimeters' information (e.g. manual change of their position if not provided with a GPS unit). The main information about turbidimeters is also shown on a map. The user can select one of the turbidimeters and specify a time window to visualize a plot of turbidity readings. Finally, Data Management Routes handle the data collection, by inserting the new sensor readings in the database. Fig. 8 shows a schematic representation of the server.

To upload the SSC readings, turbidimeters use the rsync utility, which optimizes data transfer by sending only the differences between the local and remote directories. This also takes care of the possible transient lack of connectivity, as SSC readings are stored locally by turbidimeters and then transferred at the next successful synchronization. To securely transfer the data, rsync was configured to rely on ssh. The server periodically checks the presence of updated files and stores the new values in the SQL database.

7. Discussion

The possibility of executing code written in a high-level programming language (most of the turbidimeter's logic is in Python) enables a flexible and custom collection of turbidity samples. The measuring rate is generally set using a configuration file that is provided by the coordination server. However, the configuration file can be also changed according to code that is directly executed on the turbidimeter. The measuring rate, for instance, can be dynamically adjusted according to thresholds or depending on the observed dynamics of turbidity readings. This can be particularly useful when the turbidimeter is submerged and it is not able to communicate with the external world. Let's suppose that turbidity must be sampled every 10 minutes during intense flow events, when values change more rapidly and a 1 sample per hour is deemed insufficient. According to the numbers provided in Section 4, the turbidimeter would be able to operate for approximately 6.5 days at 6 samples per hour. The turbidimeter could also be configured to operate according to two different sampling rates, one to be used during intense flow events (again 6 samples per hour) and a lower one to be used in the absence of intense flow events (let's suppose 1 sample per hour). In this case, the turbidimeter can start with the low-frequency measuring rate and then switch to high-frequency measuring only when the turbidity value becomes higher than a given threshold (because of the intense flow event). Finally, the turbidimeter could switch again to the low-sampling rate once the event is complete. If the intense flow event has a duration of two days, just as an example, the turbidimeter would be able to operate for approximately 28.8 days (3098 mAh would be spent during the two days of operation at the high-sampling rate, while the remaining 6902 mAh would be spent at the low-sampling rate). The significantly longer runtime of the smart turbidimeter can be particularly useful to cope with a possibly large number of turbidimeters to be charged, giving flexibility during in situ installation. Since Python is known by a significant fraction of scientists, not necessarily computer scientists, the use of a high-level language allows them to customize the measuring logic by themselves. Finally, since the turbidimeter runs a Linux-based operating system (Raspberry Pi OS) it is possible to remotely log into the system and update the system behavior without the need to be on-site (provided that the turbidimeter is currently connected to the Internet) or remotely execute commands on the turbidimeter. Again this possibility can be particularly useful when the number of turbidimeters to manage is relatively high, and automated operations can help avoid manual intervention. If the standard behavior of the turbidimeter, including all its configurations, is suitable for the user's needs, then no coding knowledge is required. The user just has to install the Raspberry Pi OS distribution using one of the tools provided by the Raspberry Foundation and then download the software onto the device. Configuration is stored in some text files that can be easily edited using the preferred tools.

8. Conclusion

Distributed measurements of SSC are fundamental to accurately modeling many hydro-geological phenomena, from erosion to floods. However, a distributed turbidity monitoring system requires a new generation of devices that must be cheap, flexible, and smart to cope with the different placement sites and reduce the management effort. The turbidimetry monitoring system presented in this paper has a limited cost, can be easily configured to work in mobile and fixed setups, and automatically distributes the operational parameters to remote sensors.

All the code running on the turbidimeters and on the back-end is provided according to open-source licenses and it is publicly available at the following repository:

https://github.com/alessiovecchio/turbidimeter

One of the current limitations of the system is the lack of anti-fouling techniques. Our main goal was short-term and high-frequency monitoring, to study the flash floods that develop within a few hours, which is less affected by biofouling compared to longer-term monitoring. However, when long-term studies are planned, it will be necessary to evaluate the impact of bio-fouling in the specifically considered scenario (e.g. marine vs freshwater ecosystems).

CRediT authorship contribution statement

Alessio Vecchio: Writing – review & editing, Writing – original draft, Supervision, Software, Project administration, Methodology, Investigation, Funding acquisition, Conceptualization. **Monica Bini:** Supervision, Project administration, Methodology, Funding acquisition, Data curation. **Marco Lazzarotti:** Writing – review & editing, Writing – original draft, Validation, Data curation. **Marco Luppichini:** Writing – review & editing, Validation, Data curation. **Maurizio Palmieri:** Writing – review & editing, Writing – original draft, Supervision, Software, Methodology, Investigation, Funding acquisition.

Declaration of competing interest

The authors declare that they have no known competing financial interests or personal relationships that could have appeared to influence the work reported in this paper.

Acknowledgements

Work supported by the University of Pisa (project n. PRA_2022_16 “Variazioni di frequenza delle alluvioni dell’Arno negli ultimi 3000 anni e loro effetti” CUP_I53C22001890001), and by the Italian Ministry of Education and Research (MUR) in the framework of the FoReLab project (Departments of Excellence).

Data availability

Data will be made available on request.

References

[1] J. Droujko, P. Molnar, Open-source, low-cost, in-situ turbidity sensor for river network monitoring, Sci. Rep. 12 (1) (2022) 1–13, https://doi.org/10.1038/s41598-022-14228-4.
[2] ISO, Water quality - determination of turbidity ISO 7027-1:2016, https://www.iso.org/standard/62801.html, 2016.
[3] D. Felix, I. Albayrak, R.M. Boes, In-situ investigation on real-time suspended sediment measurement techniques: turbidimetry, acoustic attenuation, laser diffraction (lisst) and vibrating tube densimetry, Int. J. Sediment. Res. 33 (1) (2018) 3–17, https://doi.org/10.1016/j.ijsrc.2017.11.003, https://www.sciencedirect.com/science/article/pii/S100162791730375X.
[4] A. Costa, D. Anghileri, P. Molnar, Hydroclimatic control on suspended sediment dynamics of a regulated Alpine catchment: a conceptual approach, Hydrol. Earth Syst. Sci. 22 (6) (2018) 3421–3434, https://doi.org/10.5194/hess-22-3421-2018, https://hess.copernicus.org/articles/22/3421/2018/.
[5] E. Skarbøvik, S. Gyritia Madsen van’t Veen, E.E. Lannergård, H. Wenng, M. Stutter, M. Bieroza, K. Atcheson, P. Jordan, J. Fölster, P.-E. Mellander, B. Kronvang, H. Marttila, Øyvind Kaste, A. Lepistö, M. Kämäri, Comparing in situ turbidity sensor measurements as a proxy for suspended sediments in North-western European streams, Catena 225 (2023) 107006, https://doi.org/10.1016/j.catena.2023.107006.
[6] A. Rymszewicz, J. O’Sullivan, M. Bruen, J. Turner, D. Lawler, E. Conroy, M. Kelly-Quinn, Measurement differences between turbidity instruments, and their implications for suspended sediment concentration and load calculations: a sensor inter-comparison study, J. Environ. Manag. 199 (2017) 99–108, https://doi.org/10.1016/j.jenvman.2017.05.017.
[7] B.G. Kitchener, J. Wainwright, A.J. Parsons, A review of the principles of turbidity measurement, Prog. Phys. Geogr. Earth Environ. 41 (5) (2017) 620–642, https://doi.org/10.1177/0309133317726540.
[8] M. Vousdoukas, S. Aleksiadis, C. Grenz, R. Verney, Comparisons of acoustic and optical sensors for suspended sediment concentration measurements under non-homogeneous solutions, J. Coast. Res. (2011) 160–164, http://www.jstor.org/stable/26482153.
[9] C.-H. Chu, Y.-X. Lin, C.-K. Liu, M.-C. Lai, Development of innovative online modularized device for turbidity monitoring, Sensors 23 (6) (2023) 1–13, https://doi.org/10.3390/s23063073.
[10] Óscar Sampedro, J.R. Salgueiro, Turbidimeter and RGB sensor for remote measurements in an aquatic medium, Measurement 68 (2015) 128–134, https://doi.org/10.1016/j.measurement.2015.02.049.
[11] F. Attivissimo, C.G.C. Carducci, A.M.L. Lanzolla, A. Massaro, M.R. Vadrucci, A portable optical sensor for sea quality monitoring, IEEE Sens. J. 15 (1) (2015) 146–153, https://doi.org/10.1109/JSEN.2014.2340437.
[12] L. Parra, J. Rocher, J. Escrivá, J. Lloret, Design and development of low cost smart turbidity sensor for water quality monitoring in fish farms, Aquac. Eng. 81 (2018) 10–18, https://doi.org/10.1016/j.aquaeng.2018.01.004.
[13] R. Sanchez, M. Groc, R. Vuillemin, M. Pujo-Pay, V. Raimbault, Development of a frugal, in situ sensor implementing a ratiometric method for continuous monitoring of turbidity in natural waters, Sensors 23 (4) (2023), https://doi.org/10.3390/s23041897.
[14] T. Matos, C.L. Faria, M.S. Martins, R. Henriques, P.A. Gomes, L.M. Goncalves, Development of a cost-effective optical sensor for continuous monitoring of turbidity and suspended particulate matter in marine environment, Sensors 19 (20) (2019), https://doi.org/10.3390/s19204439.
[15] T. Matos, J.L. Rocha, H. Dinis, C.L. Faria, M.S. Martins, R. Henriques, L. Goncalves, A low-cost, low-power and low-size multi-parameter station for real-time and online monitoring of the coastal area, in: OCEANS 2022, Hampton Roads, 2022, pp. 1–7.
[16] T. Matos, M. Martins, R. Henriques, L. Goncalves, Design of a sensor to estimate suspended sediment transport in situ using the measurements of water velocity, suspended sediment concentration and depth, J. Environ. Manag. 365 (2024) 121660, https://doi.org/10.1016/j.jenvman.2024.121660.
[17] P. Lopes, C. Penso, C. Carneiro, L. Gonçalves, Low-cost, portable in-situ spectral analysis sensor for monitoring water contamination, in: 2023 IEEE SENSORS, 2023, pp. 1–4.
[18] P. Wang, X. Wang, F. Yu, H. Gui, D. Kong, P. Khan, H. Wang, A real-time water quality measurement instrument for simultaneously detecting turbidity and particle size by using single-photon counting technique, IEEE Trans. Instrum. Meas. 71 (2022) 1–6, https://doi.org/10.1109/TIM.2022.3180421.
[19] M. Metzger, A. Konrad, F. Blendinger, A. Modler, A.J. Meixner, V. Bucher, M. Brecht, Low-cost grin-lens-based nephelometric turbidity sensing in the range of 0.1–1000 ntu, Sensors 18 (4) (2018), https://doi.org/10.3390/s18041115.
[20] Y. Wang, S.M.S.M. Rajib, C. Collins, B. Grieve, Low-cost turbidity sensor for low-power wireless monitoring of fresh-water courses, IEEE Sens. J. 18 (11) (2018) 4689–4696, https://doi.org/10.1109/JSEN.2018.2826778.
[21] J. Trevathan, W. Read, S. Schmidtke, Towards the development of an affordable and practical light attenuation turbidity sensor for remote near real-time aquatic monitoring, Sensors 20 (7) (2020), https://doi.org/10.3390/s20071993.
[22] H. Ceylan Koydemir, S. Rajpal, E. Gumustekin, D. Karinca, K. Liang, Z. Göröcs, D. Tseng, A. Ozcan, Smartphone-based turbidity reader, Sci. Rep. 9 (1) (2019) 19901, https://doi.org/10.1038/s41598-019-56474-z.
[23] T. Leeuw, E. Boss, The hydrocolor app: above water measurements of remote sensing reflectance and turbidity using a smartphone camera, Sensors 18 (1) (2018), https://doi.org/10.3390/s18010256.
[24] K. Ehmann, C. Kelleher, L.E. Condon, Monitoring turbidity from above: deploying small unoccupied aerial vehicles to image in-stream turbidity, Hydrol. Process. 33 (6) (2019) 1013–1021, https://doi.org/10.1002/hyp.13372.
[25] S. Steinbach, A. Rienow, M.W. Chege, N. Dedring, W. Kipkemboi, B.K. Thiong’o, S.J. Zwart, A. Nelson, Low-cost sensors and multitemporal remote sensing for operational turbidity monitoring in an East African wetland environment, IEEE J. Sel. Top. Appl. Earth Obs. Remote Sens. 17 (2024) 8490–8508, https://doi.org/10.1109/JSTARS.2024.3381756.
[26] K. Zhang, R.K. Amineh, Z. Dong, D. Nadler, Microwave sensing of water quality, IEEE Access 7 (2019) 69481–69493, https://doi.org/10.1109/ACCESS.2019.2918996.
[27] S. Alhaddad, M. Elerian, Mitigating suspended-sediment environmental pressure in subsea engineering through colliding turbidity currents, Results Eng. 21 (2024) 101916, https://doi.org/10.1016/j.rineng.2024.101916.
[28] J. Droujko, F. Kunz Jr, P. Molnar, Ötz-t: 3d-printed open-source turbidity sensor with Arduino shield for suspended sediment monitoring, HardwareX 13 (2023) e00395, https://doi.org/10.1016/j.ohx.2023.e00395.
[29] K. Murphy, B. Heery, T. Sullivan, D. Zhang, L. Paludetti, K.T. Lau, D. Diamond, E. Costa, N. O’Connor, F. Regan, A low-cost autonomous optical sensor for water quality monitoring, Talanta 132 (2015) 520–527, https://doi.org/10.1016/j.talanta.2014.09.045.
[30] M.A. Abid Almubaidin, S.D. Latif, K. Balan, A.N. Ahmed, A. El-Shafie, Enhancing sediment transport predictions through machine learning-based multi-scenario regression models, Results Eng. 20 (2023) 101585, https://doi.org/10.1016/j.rineng.2023.101585.
[31] K. Khairudin, A.Z. Ul-Saufie, S.F. Senin, Z. Zainudin, A.M. Rashid, N.F. Abu Bakar, M.Z. Anas Abd Wahid, S.F. Azha, F. Abd-Wahab, L. Wang, F.N. Sahar, M.S. Osman, Enhancing riverine load prediction of anthropogenic pollutants: harnessing the potential of feed-forward backpropagation (ffbp) artificial neural network (ann) models, Results Eng. 22 (2024) 102072, https://doi.org/10.1016/j.rineng.2024.102072.
[32] D. Laurent, B. Kada, B. Karenn, C. Jean-Yves, D. Mathieu, F. Bertrand, G. Celia, G. Gerard, L.B. Yves, P. Michel, R. Emmanuel, Biofouling protection by electrochlorination on optical windows for oceanographic sensors and imaging devices, in: OCEANS 2015, Genova, 2015, pp. 1–10.
[33] A. Delgado, C. Briciu-Burghina, F. Regan, Antifouling strategies for sensors used in water monitoring: review and future perspectives, Sensors 21 (2) (2021), https://doi.org/10.3390/s21020389, https://www.mdpi.com/1424-8220/21/2/389.